Cooperative Operation for Integrated Multi-Energy System Considering Transmission Losses

JINGLU LIU[ID]1, ANNA WANG1, CHONGHUI SONG[ID]1, RAN TAO2, AND XINGYU WANG1

1College of Information Science and Engineering, Northeastern University, Shenyang 110819, China
2Faculty of Engineering and Information Technologies, The University of Sydney, Sydney, NSW 2006, Australia

Corresponding author: Anna Wang (wanganna@ise.neu.edu.cn)

ABSTRACT The increasing complexity of energy internet integrated with multiple energy systems requires a more flexible energy management system. To exploit the potential of energy complementarity, maximize the consumption of renewable energy sources (RES) and minimize the operating costs, a cooperative operation model for integrated multi-energy systems (IMES) with transmission losses is proposed in this paper. On this basis, a novel multi-energy management strategy is developed to improve the energy utilization efficiency of the systems for regional operation by integrating the alternative decomposition-based decoupling method for multi-energy flow and the dynamic wolf pack algorithm (DWPA). Furthermore, the operating costs are formulated as a multi-objective optimization problem based on the Pareto efficiency to obtain more diverse solutions. Finally, case studies considered perform sensitivity analysis and demonstrate that the proposed cooperative operation model and strategy can effectively improve the economy and the flexibility of a regional energy system.

INDEX TERMS Multi-energy systems, energy complementarity, transmission loss, sensitivity, dynamic wolf pack algorithm.

NOMENCLATURE
ACRONYMS
AC	Absorption chiller
CC	Compression chiller
C-EH	Commercial energy hub
CHP	Combined heat and power
EB	Electrical boiler
EH	Energy hub
ES	Electrical storage
GB	Gas boiler
GN	Gas network
HN	Heat network
HP	Heat pump
I-EH	Industrial energy hub
IES	Integrated energy system
MILP	mix-integer linear programming
PV	Photovoltaic
R-EH	Residential energy hub
RES	Renewable energy sources
TL	Transmission loss
TS	Thermal storage
UG	Utility grid
WT	Wind turbine

PARAMETERS
η_{CHP}^{gh}	By-product heat collection efficiency of CHP
η_{CHP}^{ge}	Efficiency for power generation of CHP
η_{GB}^{gh}	Efficiency for heat generation of GB
η_{EB}^{eh}	Heat conversion efficiency of EB
η_{HP}^{ec}	Cooling efficiency of HP
η_{AC}^{hc}	Cooling coefficient of AC
η_{CC}^{ec}	Cooling conversion efficiency of CC
η_{ES}^{ch}	Charge efficiency of ES
η_{ES}^{dis}	Discharge efficiency of ES
η_{TS}^{ch}	Charge efficiency of TS
η_{TS}^{dis}	Discharge efficiency of TS

The associate editor coordinating the review of this manuscript and approving it for publication was Xiaodong Liang[ID].

VARIABLES

G Energy flow of gas
E Energy flow of electricity
H Energy flow of heat
C Energy flow of cooling
I Input of energy devices
O Output of energy devices
t Time

I. INTRODUCTION

With the growing demand of diversified energy resources and the excessive consumption of fossil fuels, the integrated energy system (IES), which is capable to coordinate diversified energy resources to generate desired energy and benefit the economy, efficiency and flexibility of the multi-energy system, has been recognized as an effective alternative to traditional energy utilization methods in the context of energy internet [1]–[4]. The complex energy couplings inside an IES are simulated by using the energy hub (EH) model [5], [6]. Compared with the individual IES, the integrated multi-energy system (IMES), which couples energy networks such as utility grid (UG), gas network (GN), heat network (HN), and several neighboring IESs, can be scheduled simultaneously to supply energy demands. Thus, the IMES can further improve the reliability and flexibility of the regional energy supply.

One of the most concerning issues is to develop a dispatch model for the IES. The objective of such a dispatch model is to minimize the IES operating costs while satisfying control constraints, such as encompassing energy balance, device capacity, ramping rate limitation, etc. [7]–[9]. Advanced modeling techniques are needed to fully simulate the energy flow inside an IES [10], [11]. The two-level economic dispatch model was proposed in Ref. [12], [13]. Ref. [12] presented the decision-making conflict among different market players. The market players must find a long-term equilibrium through price signals in a multi-energy retail market. Ref. [13] proposed a security-constrained model for integrated gas and electricity networks. The lower-level model is formulated based on Karush-Kuhn-Tucher (KKT) conditions, thus the problem can be solved by using mix-integer linear programming (MILP). Ref. [14] proposed a scenario-based stochastic IES model, an uncertainty matrix was employed to tackle the uncertainties of the RES and loads. A linear coupling matrix was proposed in Ref. [16], which facilitated the computerized calculation for an EH with arbitrary configurations. Ref. [17] proposed an optimal multi-energy flow for an IES in the carbon trading market. Ref. [20] presented a model to provide multi-energy demands and to manage continuous on/off controllable equipment. To facilitate interactions between power companies, residential buildings, and industrial consumers, a system for interconnected infrastructures based distributed multi-energy resources was established [18], [21]. A model considering energy trading between the IES and energy networks, as well as the limits

of battery systems, gas stations, and thermal storage systems, was proposed in Ref. [19]. Ref. [22] provided a flexibility assessment for IES operations. The flexibility indicator was assigned as the suppression of the uncertainty of the RES and the minimization of the operating costs. Ref. [23] investigated the effects of ice storage on the economic performance of the IES while satisfying demand response in an uncertain environment. Ref. [24] provided a management framework which consists of IES and microgrid. Moreover, the impact of the wind turbine (WT), photovoltaic (PV), and tidal generation on the planning of the IES was investigated. Ref. [25] presented an IES model that minimizes the operating costs subject to the power flow constraints and limits of technical indexes in electric vehicles (EVs) parking lots, and CHP constraints. A two-level problem for optimal day-ahead scheduling of a distribution system, which trades electricity with multiple IESs was presented in Ref. [38].

In addition to the research works that focus on the dispatch model, optimization algorithms for the operation of the IES have been proposed in some studies, such as the Monte Carlo method [26], the probability statistical method [27], the grasshopper optimization algorithm (GOA) [30], the evolutionary PSO algorithm [33] and the stochastic optimization method [28]. The ε-constraint method was employed to solve the IES coordinated operation in Ref. [15]. Ref. [29] proposed a MILP based on a multidimensional piecewise linear approximation method to calculate the optimal power flow for the IES. The proposed method can effectively solve a non-convex control problem for the gas networks. Ref. [31] introduced the coordinated scheduling strategy and a multi-objective optimization algorithm was used to obtain a Pareto optimal solution. Then the interval evidence reasoning was used to analyze the multi-attribute decision-making to determine an optimal operation solution of the IES. Ref. [32] used the distributed optimization method to find out a bargaining solution for the cooperative system ensuring the autonomous scheduling and information privacy. A decentralized algorithm was proposed in Ref. [34] to schedule the cogeneration for an IES by using the Benders decomposition. The calculation methods for the optimal IES power flow are discussed in [35]–[37]. Ref. [39] proposed a multi-objective function solving algorithm based on the tent map chaos optimization, which can reduce the operation costs and risks associated with an IES. The schedule plan of each energy device was optimized by the moth flame optimization algorithm in Ref. [40], which can effectively reduce operating costs, and the optimal output plan of each device can be obtained.

It is worth noting that most of the research works in the aforementioned literature focus on the optimal operation of a single small-scale IES. Moreover, most of the energy resources in the IES have limited capacity allocation and self-coordination capabilities. Therefore, it is difficult for a single small-scale IES to have better economic benefits. On the other hand, it is also very hard for large-scale energy storage in the IES to be fully utilized due to the high operation cost and geographical restrictions. Thus, the UG is often

used as a compensatory source to solve the power exchange problem. However, such a solution will lead to overburden and fluctuating operation for the UG. The technologies focusing on energy complementarity in the IMES can provide an innovative way to accommodate energy storage. This local community as a local energy resource can ease the cooperative operation of IESs.

To exploit the potential of the multi-energy complementarity among various IESs and achieve higher efficiency, this paper develops a cooperative operation IMES based on the EH concept and proposes a cooperation based control strategy. The main contributions are summarized as follows:

1) Based on the linearized coupling matrix of the EH model, a cooperative operation model is presented for the IMES to combine the residential EH (R-EH), the commercial EH (C-EH), the industrial EH (I-EH), the UG, the GN and the HN. Furthermore, the transmission losses is developed, which can further study the actual supply-demand balance and avoid serious economic losses.

2) The operating costs are formulated as a multi-objective optimization problem based on the Pareto efficiency to obtain more diverse solutions.

3) A novel multi-energy management strategy that integrates the alternative decomposition-based decoupling method of multi-energy flow and the dynamic wolf pack algorithm (DWPA) has been further developed.

4) The DWPA is presented, where dynamic scout direction, Fibonacci sequence, avoiding inferiority, and Levy-flight function are introduced as an improved function. Compared with other algorithms, the DWPA has advantages in terms of operating costs and time.

5) The case studies demonstrate that, compared to the non-cooperative mode, the proposed control strategy can achieve better cost-effective performance. Whilst, the sensitivity analysis is performed to explore the impact of the confidence of the objective function and constraints on the operation of IMES.

The rest of the paper is arranged as follows. Section II presents the coupling model for EH, the energy network models, and the cooperative operation model for the IMES. The proposed multi-energy management strategy is introduced in Section III. Section IV demonstrates the case studies and the effectiveness of the proposed strategy, while Section V concludes the paper.

II. MODELING APPROACH FOR THE IMES

A. LINEARIZED COUPLING MODEL OF EH

The flexibility of the EH mainly comes from the devices and the bifurcations of energy flows. Fig. 1 illustrates the topology of a typical EH, which consists of a combined heat and power (CHP), an electric boiler (EB), a gas boiler (GB), a compression chiller (CC), an absorption chiller (AC), an electrical storage (ES) and a thermal storage (TS).

The linearized coupling relationship for the EH can be expressed according to the energy efficiency matrix (1), as shown at the bottom of the next page. The energy
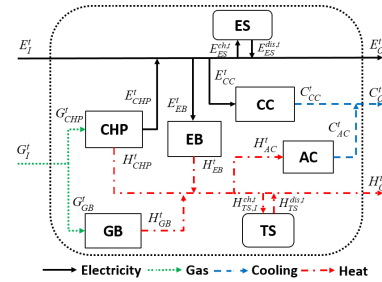

FIGURE 1. The topology of a typical EH.

inputs E_I^t, G_I^t are bought from the UG and the GN, while the outputs E_O^t, H_O^t, C_O^t are electricity, heat, and cooling demands, which can be met by coordinating different resources. The inlets for different energy devices are G_{CHP}^t, G_{GB}^t, E_{EB}^t, E_{CC}^t, H_{AC}^t, $E_{ES,I}^{ch,t}$, $E_{ES,I}^{dis,t}$, $H_{TS,I}^{ch,t}$, and $H_{TS,I}^{dis,t}$. The outlets from different energy devices are E_{CHP}^t, H_{CHP}^t, H_{GB}^t, H_{EB}^t, C_{CC}^t, C_{AC}^t, $E_{ES,O}^{ch,t}$, $E_{ES,O}^{dis,t}$, $H_{TS,O}^{ch,t}$, and $H_{TS,O}^{dis,t}$. η_{CHP}^{gh}, η_{CHP}^{ge}, η_{GB}^{gh}, η_{EB}^{eh}, η_{HP}^{ec}, η_{AC}^{hc}, η_{CC}^{ec}, η_{ES}^{ch}, η_{ES}^{dis}, η_{TS}^{ch}, and η_{TS}^{dis} are the conversion efficiencies of energy devices, respectively.

The cooperative operation model for the IMES is shown in Fig. 2, which couples five EHs, a UG, a GN, and a HN.
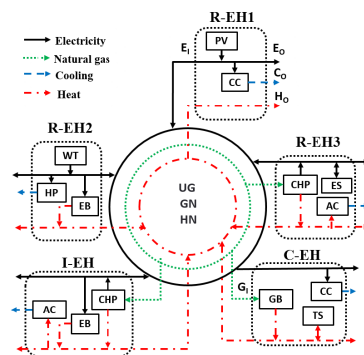

FIGURE 2. The cooperative operation model for the IMES.

As shown in Fig. 2, the IMES contains multiple EHs and the R-EH1 contains the PV, and the CC; the R-EH2 consists of the WT, the HP, and the EB; the R-EH3 contains the CHP, the AC, and the ES; the I-EH consists of the CHP, the EB, and the AC; and the C-EH contains the GB, the CC, and the TS. The surplus energy resources can be locally shared between the EHs to supply energy demands. This cooperative operation model can be extended to a very big network with numerous EHs.

B. UG MODEL

In the IMES, the UG can be modeled using an optimal power flow model [41]. The integration of RES and energy coupling makes the power flow more complicated.

The relevant calculations can be expressed as

$$P_n = V_n \sum_{m \in n}^{N} V_m (G_{n,m} \cos \theta_{n,m} + B_{n,m} \sin \theta_{n,m}) \quad (2)$$

$$Q_n = V_n \sum_{m \in n}^{N} V_m (G_{n,m} \sin \theta_{n,m} - B_{n,m} \cos \theta_{n,m}) \quad (3)$$

where $P_n(Q_n)$ is the active (reactive) power injection of the node n; V_n is the voltage amplitude of the node n; V_m is the voltage amplitude of the node m; $\theta_{n,m}$ is the phase difference between the node n and m; $G_{n,m}$ is the conductance; $B_{n,m}$ is the susceptance; N is the node number.

The node energy balance and power flow constraints can be described as

$$\begin{cases} \sum_{m \in n} P_{n,m} = P_n \\ \sum_{m \in n} Q_{n,m} = Q_n \end{cases} \quad (4)$$

$$\begin{cases} P_n^{\min} \leq P_n \leq P_n^{\max} \\ Q_n^{\min} \leq Q_n \leq Q_n^{\max} \\ V_n^{\min} \leq V_n \leq V_n^{\max} \\ P_{n,m} \leq P_{n,m}^{\max} \\ Q_{n,m} \leq Q_{n,m}^{\max} \end{cases} \quad (5)$$

where $P_{n,m}(Q_{n,m})$ is the active (reactive) power of the power line between the node n and m; $P_{n,m}^{\max}$ ($Q_{n,m}^{\max}$) is the transmission power constraints of the power line; $P_n^{\max}, P_n^{\min}, Q_n^{\max}, Q_n^{\min}, V_n^{\max}, V_n^{\min}$ are the upper and lower limits of the active power, reactive power and voltage amplitude, respectively.

The voltage stability constraints can be described as

$$\left| \frac{V_n - V_{ref}}{V_{ref}} \right| < THR \quad (6)$$

where V_{ref} is the reference voltage value; THR is the threshold, which limits the allowable voltage range

C. GN MODEL

The model for gas flow balance can be formulated as

$$A_G F = G \quad (7)$$

$$A_{G,kl} = \begin{cases} 1 & \text{gas flow into node } k \text{ from pipe } l \\ -1 & \text{gas flow out of node } k \text{ from pipe } l \\ 0 & \text{no flow between node } k \text{ and pipe } l \end{cases} \quad (8)$$

where A_G is the node-branch incidence matrix; F is the gas flow in the pipe; G is the gas injection of the node.

The relationship between gas flow and node pressure can be described as [42].

$$f_{k,\rho} = 5.72 \times 10^{-4} \sqrt{(\Delta \kappa_{k,\rho}) d^5 / \vartheta L \nu} \quad (9)$$

where $f_{k,\rho}$ is the gas flow in the pipe between node k and node ρ; $\Delta \kappa_{k,\rho}$, ϑ are the pressure drop and friction factor of the pipe; d, L are the diameter and length of the pipe; ν is the specific gravity of the gas.

The node flow balance, node flow and pressure constraints can be expressed as

$$\sum f_{k,\rho} = f_\rho \quad (10)$$

$$\begin{cases} f_\rho^{\min} \leq f_\rho \leq f_\rho^{\max} \\ p_\rho^{\min} \leq p_\rho \leq p_\rho^{\max} \end{cases} \quad (11)$$

where f_ρ is the flow of the node ρ; p_ρ is the pressure of the the node ρ; $f_\rho^{\max}, f_\rho^{\min}, p_\rho^{\max}, p_\rho^{\min}$ are the upper and lower limits of the flow and pressure, respectively.

D. HN MODEL

Generally, the HN model can be divided into two parts: the hydraulic circuit and the thermal circuit. The hydraulic circuit can be modeled as [43]

$$A_H \Pi = M_k \quad (12)$$

$$BR\Pi |\Pi| = \sum_{j=1}^{N} B_{i,j} R_j \Pi_j |\Pi_j| = 0 \quad (13)$$

$$
\begin{bmatrix}
E_O^t \\ H_O^t \\ C_O^t \\ E_{CHP}^t \\ H_{CHP}^t \\ H_{GB}^t \\ H_{EB}^t \\ C_{CC}^t \\ C_{AC}^t \\ E_{ES,O}^{ch,t} \\ E_{ES,O}^{dis,t} \\ H_{TS,O}^{ch,t} \\ H_{TS,O}^{dis,t}
\end{bmatrix}
=
\begin{bmatrix}
1 & \eta_{CHP}^{ge} & 0 & -1 & -1 & 0 & \eta_{ES}^{ch} & -\eta_{ES}^{dis} & 0 & 0 \\
0 & \eta_{CHP}^{gh} & \eta_{GB}^{gh} & \eta_{EB}^{eh} & 0 & -1 & 0 & 0 & \eta_{TS}^{ch} & -\eta_{TS}^{dis} \\
0 & 0 & 0 & 0 & \eta_{CC}^{ec} & \eta_{AC}^{hc} & 0 & 0 & 0 & 0 \\
0 & \eta_{CHP}^{ge} & 0 & 0 & 0 & 0 & 0 & 0 & 0 & 0 \\
0 & \eta_{CHP}^{gh} & 0 & 0 & 0 & 0 & 0 & 0 & 0 & 0 \\
0 & 0 & \eta_{GB}^{gh} & 0 & 0 & 0 & 0 & 0 & 0 & 0 \\
0 & 0 & 0 & \eta_{EB}^{eh} & 0 & 0 & 0 & 0 & 0 & 0 \\
0 & 0 & 0 & 0 & \eta_{CC}^{ec} & 0 & 0 & 0 & 0 & 0 \\
0 & 0 & 0 & 0 & 0 & \eta_{AC}^{hc} & 0 & 0 & 0 & 0 \\
0 & 0 & 0 & 0 & 0 & 0 & \eta_{ES}^{ch} & 0 & 0 & 0 \\
0 & 0 & 0 & 0 & 0 & 0 & 0 & -\eta_{ES}^{dis} & 0 & 0 \\
0 & 0 & 0 & 0 & 0 & 0 & 0 & 0 & \eta_{TS}^{ch} & 0 \\
0 & 0 & 0 & 0 & 0 & 0 & 0 & 0 & 0 & -\eta_{TS}^{dis}
\end{bmatrix}
\begin{bmatrix}
E_I^t \\ G_{CHP}^t \\ G_{GB}^t \\ E_{EB}^t \\ E_{CC}^t \\ H_{AC}^t \\ E_{ES,I}^{ch,t} \\ E_{ES,I}^{dis,t} \\ H_{TS,I}^{ch,t} \\ H_{TS,I}^{dis,t}
\end{bmatrix}
\quad (1)
$$

$$A_{H,kl} = \begin{cases} 1 & \text{water flow into node } k \text{ from pipe } l \\ -1 & \text{water flow out of node } k \text{ from pipe } l \\ 0 & \text{no flow between node } k \text{ and pipe } l \end{cases}$$

$$(14)$$

where A_H is the node-branch incidence matrix; Π is the water flow of the pipe; M_k is the water flow of the node; i is the loop label; j is the pipe label; B is the loop incidence matrix; R is the resistance coefficient.

The thermal circuit can be formulated as

$$Q_k = C_H m_k (T_k^I - T_k^O) \tag{15}$$

$$T_{out} = (T_{in} - T) e^{-\varpi L / C_H \Pi} + T \tag{16}$$

$$\sum_{\varsigma \in k} \left(m_\varsigma^I T_\varsigma^I \right) = \left(\sum_{\varsigma \in k} m_\varsigma^O \right) T_\varsigma^O \tag{17}$$

where Q_k is the heat energy of node k; C_H is the specific heat capacity; L is the length of the pipe; m_k is the water flow of node k; T is the ambient temperature; T_k^I, T_k^O are the inlet and outlet temperature of the node k; T_{in}, T_{out} are the inlet and outlet temperature of the pipe; $T_\varsigma^I, m_\varsigma^I$ are the temperature and water flow into the node from the pipe ς; $T_\varsigma^O, m_\varsigma^O$ are the temperature and water flow out of the node from the pipe ς; ϖ is the thermal conductivity.

E. TRANSMISSION LOSS
To address the energy complementarity between different EHs, the distance between EH i and j is donated as $L_{i,j}$. The power transmission losses E_{loss} and the heat transmission losses H_{loss} of $L_{i,j}$ that can be expressed by [47], [48]

$$\begin{cases} E_{loss} = \sum_{i=1}^{N} P_i^2 B_i = \sum_{i=1}^{N} P_i^2 \dfrac{\rho_r}{U_r^2 S_r} L_{i,j} \\ H_{loss} = 2\pi \dfrac{T_{w,k} - T_{avg,\varsigma}}{\sum R_h} L_{i,j} \end{cases} \tag{18}$$

where P_i is the electricity output of the EH i; B_i is the loss coefficient; ρ_r is the resistivity; U_r^2 is the rated voltage; S_r is the cross-sectional area of the resistance; $\sum R_h$ is the thermal resistance of the pipe per kilometer from the heat medium to the surrounding medium; $T_{w,k}$ is the supply-water temperature at node k; $T_{avg,\varsigma}$ is the mean temperature of the medium around the pipe ς. Assuming that the characteristics of the power lines among EHs are the same, thus the energy loss is proportional to the length $L_{i,j}$.

III. CO-SCHEDULING METHOD
A. OBJECTIVE FUNCTION
To fulfill control demands for different energy resources simultaneously and achieve the minimum operating costs f_{day} for the IMES, the objective function is formulated as

$$\begin{cases} f_{day} = \alpha_{f_1} f_1 + \beta_{f_2} f_2 \\ f_1 = \sum_{t=1}^{T=24} \left[\lambda_{E,net}^t E_{net}^t + \lambda_{G,net} G_{net}^t + \lambda_{H,net} H_{net}^t \right] \\ f_2 = \sum_{t=1}^{T=24} \left[\chi_G G_{CHP}^t + \chi_G G_{GB}^t \right] \end{cases} \tag{19}$$

where f_1 is the cost of the energy procurement; $\lambda_{E,net}^t, \lambda_{G,net}, \lambda_{H,net}$ are the prices for purchasing electricity, gas, and heat, respectively; E_{net}^t, G_{net}^t and H_{net}^t are the energy procurements from the UG, the GN, and the HN; f_2 is the environmental costs; $\alpha_{f_1}, \beta_{f_2}$ are the weight coefficients; χ_G is the penalty factors.

The probabilistic constraints can be described as

$$\Pr \left\{ \bar{f}_{day} \right\} \geq \partial \tag{20}$$

where ∂ is the confidence of the objective function; $\bar{f}_{day}$ is the objective function when the confidence is ∂.

B. OPERATIONAL CONSTRAINTS
The energy balance for all resources in the IMES can be described as

$$E_{EH}^t + \sum E_{HP}^t + \sum E_{CC}^t + \sum E_{EB}^t + \sum E_{ES}^{ch,t} + \sum_{j:j \neq i} E_{i,j}^t$$

$$= E_{net}^t + \sum E_{PV}^t + \sum E_{WT}^t + \eta_{CHP}^{ge} \sum G_{CHP}^t$$

$$+ \sum E_{ES}^{dis,t} + \sum_{i:i \neq j} E_{j,i}^t \tag{21}$$

$$H_{EH}^t + \sum H_{AC}^t + \sum H_{TS}^{ch,t} + \sum_{j:j \neq i} H_{i,j}^t$$

$$= \eta_{CHP}^{gh} \sum G_{CHP}^t + \sum H_{TS}^{dis,t} + H_{net}^t + \eta_{GB}^{gh} \sum G_{GB}^t$$

$$+ \eta_{EB}^{eh} \sum E_{EB}^t + \sum_{i:i \neq j} H_{j,i}^t \tag{22}$$

$$C_{EH}^t$$

$$= \eta_{AC}^{hc} \sum H_{AC}^t + \eta_{HP}^{ec} \sum E_{HP}^t + \eta_{CC}^{ec} \sum E_{CC}^t \tag{23}$$

where $E_{i,j}^t, H_{i,j}^t$ are the exchanged electricity and heat energy between EH i and j; (21) describes the balance of the electricity, (22) formulates the balance of heat energy, and (23) calculates the balance of cooling energy.

The probabilistic constraints can be expressed as

$$\begin{cases} \Pr \left\{ -\zeta_1 \leq E_{i,j}^t \leq \zeta_1 \right\} \geq \phi \\ \Pr \left\{ -\zeta_2 \leq H_{i,j}^t \leq \zeta_2 \right\} \geq \phi \end{cases} \tag{24}$$

where ϕ is the confidence of the constraints; ζ_1, ζ_2 are the maximum exchanged energy

The CHP needs to meet the operational constraints and the ramping rate limitation, which can be described as

$$\begin{cases} E_{CHP}^{mid} \leq E_{CHP}^t + \dfrac{E_{CHP}^{mid} - E_{CHP}^{\min}}{Q_{CHP}^{mid}} Q_{CHP}^t \leq E_{CHP}^{\max} \\ 0 \leq \lambda_m Q_{CHP}^t - E_{CHP}^t \leq \lambda_m Q_{CHP}^{mid} - E_{CHP}^{\min} \end{cases} \tag{25}$$

$$\begin{cases} E_{CHP}^{down} \Delta t \leq E_{CHP}^t - E_{CHP}^{t-1} \leq E_{CHP}^{up} \Delta t \\ Q_{CHP}^{down} \Delta t \leq Q_{CHP}^t - Q_{CHP}^{t-1} \leq Q_{CHP}^{up} \Delta t \end{cases} \tag{26}$$

where Q_{CHP}^{mid} is the heat energy output when the power generation of the CHP is $E_{CHP}^{\min}$; $E_{CHP}^{\max}$ is the maximum power generation; E_{CHP}^{mid} is the minimum power generation of the CHP; λ_m

is the electro-thermal elastic coefficient; E_{CHP}^{up}, E_{CHP}^{down} (Q_{CHP}^{up}, Q_{CHP}^{down}) are the upper and lower limits of increase and decrease of electricity (heat) per unit time; Δt is the ramp response time.

The energy devices must operate within its rated capacity. Their capacity limits are formulated as

$$E_{HP}^{\min} \leq E_{HP}^t \leq E_{HP}^{\max} \tag{27}$$

$$E_{EB}^{\min} \leq E_{EB}^t \leq E_{EB}^{\max} \tag{28}$$

$$G_{GB}^{\min} \leq G_{GB}^t \leq G_{GB}^{\max} \tag{29}$$

$$E_{CC}^{\min} \leq E_{CC}^t \leq E_{CC}^{\max} \tag{30}$$

$$E_{AC}^{\min} \leq E_{AC}^t \leq E_{AC}^{\max} \tag{31}$$

$$E_{ES}^{dis,\min} \leq E_{ES}^{dis,t} \leq E_{ES}^{dis,\max} \tag{32}$$

$$E_{ES}^{ch,\min} \leq E_{ES}^{ch,t} \leq E_{ES}^{ch,\max} \tag{33}$$

$$H_{TS}^{dis,\min} \leq H_{TS}^{dis,t} \leq H_{TS}^{dis,\max} \tag{34}$$

$$H_{TS}^{ch,\min} \leq H_{TS}^{ch,t} \leq H_{TS}^{ch,\max} \tag{35}$$

The energy storage devices are constrained by the state of charge (SOC), which can be obtained as

$$SOC_{ES}^{\min} \leq SOC_{ES}^t \leq SOC_{ES}^{\max} \tag{36}$$

$$SOC_{ES}^t = SOC_{ES}^{t-1} + \left(\eta_{ES}^{ch} E_{ES}^{ch,t} - \eta_{ES}^{dis} E_{ES}^{dis,t}\right)\Delta t \tag{37}$$

$$SOC_{TS}^{\min} \leq SOC_{TS}^t \leq SOC_{TS}^{\max} \tag{38}$$

$$SOC_{TS}^t = SOC_{TS}^{t-1} + \left(\eta_{TS}^{ch} H_{TS}^{ch,t} - \eta_{TS}^{dis} H_{TS}^{dis,t}\right)\Delta t \tag{39}$$

where $SOC_{ES}^{\max}$, $SOC_{ES}^{\min}$, $SOC_{TS}^{\max}$, $SOC_{TS}^{\min}$ are the upper and lower limits of ES and TS capacities, respectively; Δt is the charge/discharge time.

C. DWPA
The proposed IMES model requires compliance with various non-linear operational constraints. However, the increasing system complexity brings considerable computational requirements to traditional approaches, making them technically less appealing. Besides, with the increasing scale of future IMES, the traditional approaches will face a series of problems, such as lower converging speed or deviation from the global optima. On the other hand, novel intelligent meta-heuristic algorithms have been employed to solve different economic dispatch problems and achieved satisfactory results [30], [33], [44]. In this section, a power flow optimization method based on DWPA is proposed to optimize the operation and dispatch the energy resources within the IMES. The wolf pack algorithm (WPA) selects the best wolf as the lead wolf, and then, the WPA divides other wolves into the scout wolves and ferocious wolves [44]. The prey behaviors include scout, summon, siege, and renew. The lead wolf summons the wolves to capture the prey according to the prey odor smelled from the scout wolves.

We first define $\mathbf{x}_{1\times H}$ as the position of any wolf and it can be used as inputs for the objective function. The position

$\mathbf{x}_{1\times H}$ can be formulated as

$$
\begin{aligned}
\mathbf{x}_{1\times H} &= [x_1, x_2, \cdots, x_H] \\
&= \left[G_{CHP1}^t, G_{CHP2}^t \cdots, G_{GB1}^t, G_{GB2}^t, \cdots, E_{CC1}^t, E_{CC2}^t, \cdots\right]
\end{aligned} \tag{40}
$$

where the associated costs f_{day} calculated using (19) is defined as the fitness value for $\mathbf{x}_{1\times H}$.

The scout wolves explore the environment to hunt for the prey. The $x_{i,h}^\alpha$ can be updated by [44]

$$x_{i,h}^\alpha = x_{i,h} + \sin(2\pi \times \alpha/s)\tau_h^a \tag{41}$$

where $\alpha = (1, 2, \cdots, s)$ denotes the prey direction; τ_h^a is the scout step; s is the scout direction; $x_{i,h}$ represents the position of the i-th scout wolf in the h-th dimension $h = (1, 2 \cdots, H)$, which corresponds to the electricity, gas, and heat energy procurements.

However, the basic WPA will use a fixed s that leads to insufficient diversity and randomness. In order to improve the global search efficiency, a dynamic scout direction is proposed in this paper and the new scout behavior can be updated as

$$I_h = diag(1, 1, \ldots, 1) \tag{42}$$

$$s_{2h} = [I_h; -I_h] \tag{43}$$

$$s_{2h}(\ell) = [s_{l,1}, s_{l,2}, \cdots, s_{l,H}], \quad \ell = (1, 2, \cdots 2H) \tag{44}$$

$$x_{i,h}^\alpha = x_{i,h} + s_{2h}(\ell) \times \tau_h^a \tag{45}$$

where I_h is an identity matrix of scout direction in the h-th trace; s_{2h} is the dynamic scout direction.

If the fitness value of the i-th scout wolf is greater than the lead wolf, the scout wolf will replace the lead wolf and summon other wolves. The position of the ferocious wolf can be updated as

$$x_{i,h}^{j+1} = x_{i,h}^j + w(g_h^j - x_{i,h}^j)\tau_h^b / \left|g_h^j - x_{i,h}^j\right| \tag{46}$$

where $w \in [0, 1]$ is the odor weight; τ_h^b indicates the raid step; $x_{i,h}^{j+1}$ is the position of the i-th ferocious wolf at the $j+1$ iteration, g_h^j is the position of the lead wolf.

The step size of the ferocious wolf will be slowly reduced to approach the lead wolf. The siege radius is defined as

$$\psi = \sum_{h=1}^{H} \left|\xi_h^{\max} - \xi_h^{\min}\right|/(H\varepsilon) \tag{47}$$

where ε is the i-th distance determinant coefficient; ψ is the distance between the ferocious wolf and the lead wolf when initiating the siege behavior; $\xi_h^{\max}$ and $\xi_h^{\min}$ are upper and lower values.

The siege behavior is formulated as [44]

$$x_{i,h}^{j+1} = x_{i,h}^j + \gamma \left|g_h^j - x_{i,h}^j\right|\tau_h^c \tag{48}$$

where τ_h^c is the siege step and $\gamma \in [-1, 1]$. If the fitness value of the i-th ferocious wolf is better than the lead wolf, the lead wolf will be replaced.

The basic WPA uses a fixed step to update the scout wolf position and if the scout step is too large, the convergence precision will be attenuated. However, if the scout step is too small, it will slow down the convergence speed. To balance the convergence precision and speed, a dynamic scout step based on the Fibonacci sequence $F_j = [(1 + \sqrt{5}/2)^j - (1 - \sqrt{5}/2)^j]/\sqrt{5}$ is formulated as

$$\tau_h^a = \chi F_j^{1/F_j} \tau_h^a \tag{49}$$

where $\chi > 1$ is the learning rate.

In the context of the basic WPA, only the lead wolf has affects on the siege behavior of the whole wolf pack. However, in the DWPA, ferocious wolves can interact with each other and the siege behavior of the wolf pack will be updated using interactions from all ferocious wolves. The intention for that is to quickly escape from the area where it has a lower probability for the optimal prey. Therefore, the proposed avoiding inferiority can improve the convergence speed. The pseudo-code is given as follows.

Pseudo-code for Avoiding Inferiority

---

1. **for** each ferocious wolf i
2.   **if** the distance between the ferocious wolf i and the lead wolf is smaller than ψ
3.   Run with step size τ_h^c using (48).
4.   **if** the distance between the ferocious wolf i and another wolf with the poorer fitness value is smaller than ψ in (47).
5.   Run with a relatively large step size τ_h^b using (46).
6.   **else**
7.   Run with step size τ_h^c using (48).
8.   **end**
9.   **end**
10. **end for**

To avoid premature convergence, σ wolves which have relatively lower fitness will be renewed to maintain the diversity of the wolf pack. σ is a random value between $[n/2\delta, n/\delta]$, where δ is the population renewing proportional coefficient. The Levy-flight [45] is also taken to enhance the diversity, which can be attained as

$$Levy(\beta)$$
$$= \mu \varphi / |v|^{1/\beta} \tag{50}$$
$$\varphi = \left[\Gamma(1 + \beta) \sin(\pi\beta/2)/(\Gamma((1 + \beta)/2)2^{(\beta-1)/2}\beta) \right]^{1/\beta} \tag{51}$$
$$x_{i,h}^{j+1} = x_{i,h}^j + r \oplus levy(\beta) \tag{52}$$

where $\beta \in [0, 2]$ is a fixed number and used to adjust the stability; μ, v are normal distributions; r is a random number between $[0,1]$; Γ is the Gamma function.

D. DECOUPLING METHOD

The implementation flowchart for the decoupling method for the IMES is shown in Fig. 3. The traditional energy flow calculation method, such as the Newton Raphson method [43],
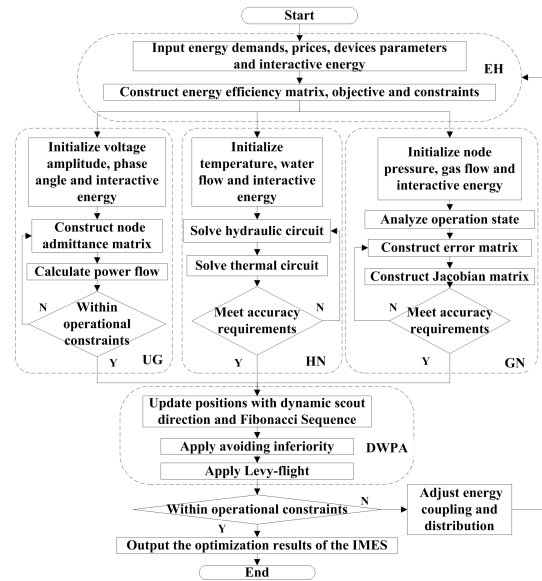

FIGURE 3. The optimization flowchart for the IMES.

needs to consider different system components (e.g., the UG, the GN, the HN, and the EH) as a whole, which complicates the calculation and increases the dimension of the system equations. The proposed IES model only considers the energy efficiency matrix calculation of the EH. Therefore, an alternative decomposition-based decoupling method can be applied for the optimal interaction of EHs and energy networks [46]. The decoupling method can calculate the energy flow for the UG, the GN, and the HN, respectively. Thus, a more accurate dispatch for the multi-energy flow can be obtained.

IV. RESULTS AND DISCUSSION

A. CASE SETTINGS

To demonstrate the effectiveness of the day-ahead IMES model and the proposed method, a test system is developed which consists of a UG (e.g., an IEEE 33-bus system), a GN (e.g., a 9-node low-pressure gas system), the HN (e.g., a 6-node heat system) and 5 EHs, as depicted in Fig 4. The EHs cover an urban area which consists of 1800 residences, 10 commercial units, and two industrial units. The Node E5, E13, E20, E23, and E30 are the coupling points between the UG and the EHs. The Node G2, G7, and G9 from the GN are connected to the R-EH3, the I-EH, and the C-EH, respectively. Except for the Node H1 of the HN, each network node of the HN is connected to one EH. It is assumed that the maximum heat loss in water pipe is 10%, the allowable voltage range is [0.95p.u. 1.05p.u.] and the allowable pressure range is [0.9p.u. 1.1p.u.].

Fig. 5(a), (b), (c) show the data for the energy demands of 5 EHs. The hourly outputs of the RES are obtained from day-ahead forecasts, as shown in Fig. 6(a). The curves of time-of-use price for electricity, natural gas, and hot water are shown in Fig. 6(b). The parameters of energy devices are listed in Table 1-2.
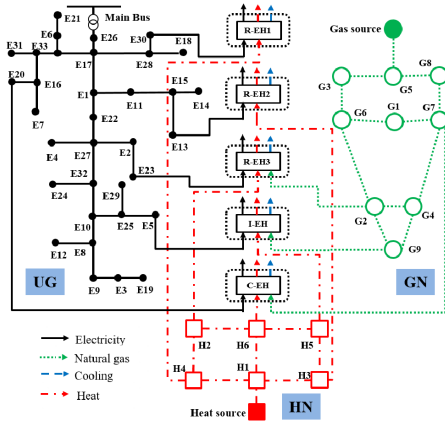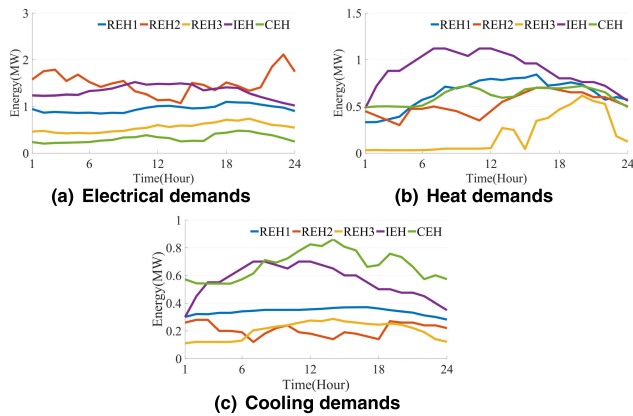
FIGURE 4. The proposed IMES model.

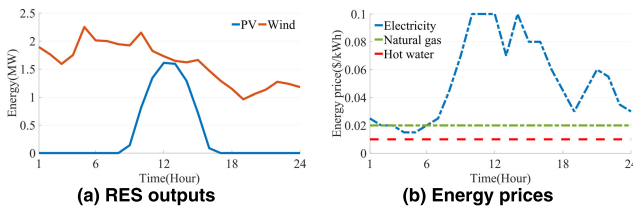**FIGURE 5.** Daily energy demands of the IMES.

FIGURE 6. Hourly RES outputs and energy prices.

TABLE 1. Parameters of energy conversion devices in IMES.

Component	Capacity (MWh)	Efficiency
CHP	$G_{CHP}^{max} = 0.5$	$\eta_{CHP}^{ge} = 0.3\,\eta_{CHP}^{gh} = 0.45$
HP	$E_{HP}^{max} = 0.2$	$\eta_{HP}^{ec} = 2$
CC	$E_{CC}^{max} = 0.2$	$\eta_{CC}^{ec} = 3$
GB	$G_{GB}^{max} = 0.9$	$\eta_{GB}^{gh} = 0.8$
EB	$E_{EB}^{max} = 0.3$	$\eta_{EB}^{eh} = 0.9$
AC	$H_{AC}^{max} = 0.5$	$\eta_{AC}^{hc} = 0.7$
ES	$E_{ES}^{max} = 0.2$	$\eta_{ES}^{ch} = 0.75, \eta_{ES}^{dis} = 0.75$
TS	$H_{TS}^{max} = 0.25$	$\eta_{TS}^{ch} = 0.8, \eta_{TS}^{dis} = 0.8$

TABLE 2. Rated capacities of energy devices.

EH	Device	Number	Capacity (MWh)
R-EH1	PV	16	0.1
	CC	1	0.2
R-EH2	WT	20	0.12
	HP	1	0.2
	EB	1	0.3
R-EH3	CHP	4	0.5
	AC	1	0.5
	ES	10	0.2
I-EH	CHP	10	0.5
	EB	3	0.3
	AC	2	0.5
C-EH	GB	3	0.9
	CC	2	0.2
	TS	10	0.25
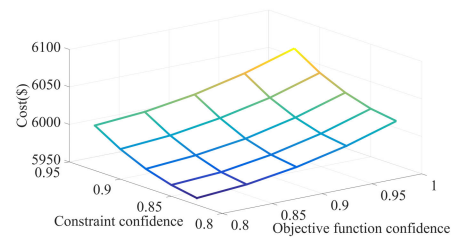
FIGURE 7. The relationship between the cost and confidence.

B. SENSITIVITY ANALYSIS AND PARETO FRONT

In order to compare the operating results, the total operating costs of the IMES under different confidence values of the objective function and constraint are selected.

As shown in Fig. 7, with the increase in the confidence value of the objective function and constraint, the operating costs of the IMES increase. It is demonstrated that as the confidence value increases, the uncertainty input is suppressed, the reliability requirements of the objective functions and constraints of the IMES will increase, and the reliability will be compensated with a higher operating cost.

To further explain the Pareto efficiency in IMES models, the Pareto optimal sets of costs are compared with other methods. The weights α_{f_1}, β_{f_2} are set to $\alpha_{f_1} \in [0:0.02:1]$, and $\beta_{f_2} \in [1:0.02:0]$.

As shown in Fig. 8, the Pareto optimal sets can effectively reflect the relationship between the energy purchase costs and environmental costs. The point A indicates that the energy purchase costs are dominant, that is, the weight of the energy purchase costs is higher than that of the environmental costs. The point B indicates that the environmental costs are dominant. Other points can be served as the compromise solutions for decision-makers under different environmental and economic requirements. When the energy purchase costs decrease, the environmental costs increase.

C. OPERATIONAL SCHEDULING FOR THE IMES

Simulation results are summarized in Fig. 9 to show how the energy distribution, and conversion within the IMES. The objective function confidence and constraints confidence are both set to 0.9. The weight coefficients are both set to 0.5.
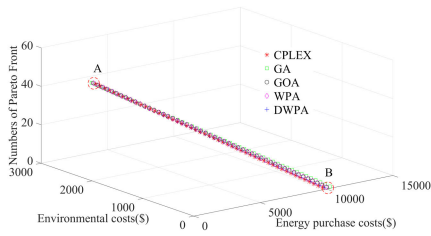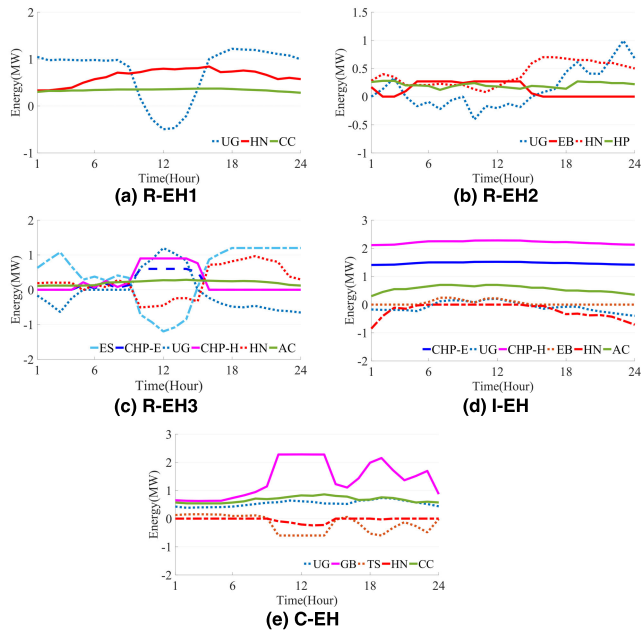
FIGURE 8. Pareto front curve.

FIGURE 9. The energy devices in the IMES.

With the expansion of energy couplings and complementarities, it is necessary to analyze the operational scheduling of different energy devices.

The electrical loads of the R-EH1 are mainly supplied by the PV and UG. The excess PV power can send to other EHs. Because the R-EH1 doesn't own any thermal supply, it needs to obtain heat energy from other EHs, as shown in Fig. 9 (a). Since the electricity produced by the WT is sufficient in R-EH2, it will be converted to heat and cooling energy, as depicted in Fig. 9 (b). It is cost-effective to purchase electricity from UG to supply electrical loads due to the lower price during the evening. In the cooperative mode, the ES is heavily used because it is efficient to charge or discharge to accommodate the fluctuations of the RES, as illustrated in Fig. 9 (c). For the I-EH, the electrical load is mainly supplied by the CHP, as shown in Fig. 9 (d). The extra heat generated by the CHP will be sent to other EHs. The EB can be used as an auxiliary heat source. The cooperative operation improves the operating efficiency of the CHP, which leads to an increase in gas consumption. Moreover, it is more cost-effective to choose the AC over the CC for supplying cooling loads because the AC can use the extra heat to supply cooling loads. The electrical loads in the C-EH can be

supplied by the surplus electricity from other EHs, which can reduce the power procurement from the UG, as depicted in Fig. 9 (e). The TS is fully utilized to store the extra heat generated by the GB, which improves the system flexibility to handle the heat supply.

D. COMPARISON WITH OTHER METHODS

The computational results are given in Fig. 10 and Table 3. The result shows that in terms of solution quality, the DWPA can provide a sub-optimal solution that is very close to the optimal value obtained by CPLEX [13]. However, the CPLEX requests a longer time to solve the economic dispatch problem. Compared with the genetic algorithm (GA) [39], the GOA [30], and the WPA [44], the proposed DWPA can reduce the operating costs by 1.96%, 0.74% and 0.55%, respectively, which illustrates that the proposed method has better global search capability and convergence performance than other methods within a shorter computational time.
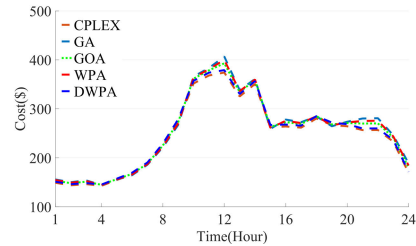

FIGURE 10. Operating costs of different methods.

TABLE 3. Results obtained from different methods.

Methods	$f_{day}(\$)$	Time(s)
CPLEX	5944.87	2653.28
GA	6086.35	83.67
GOA	6013.53	156.86
WPA	6002.08	160.33
DWPA	5969.31	126.25

E. ENERGY COMPLEMENTARITY IN THE IMES

The simulation results of the energy procurements (e.g., electricity, gas, heat) of the IMES with or without cooperation are shown in Fig. 11 and the detailed operating costs are compared in Table 4. The results show that, compared with the non-cooperation mode, the IMES with cooperation needs lower electricity and heat procurements. The gas procurement is increased due to the increased operating efficiency of the CHP. When operating under cooperation mode, the IMES has more flexibility, which means the proposed model is capable of utilizing different energy devices to flexibly deal with the diversified energy resources to fulfill desired energy demands. The internal energy exchange among different EHs can lower the electricity purchase from the UG, which reduces the burden of the UG power. It can be concluded that the EHs of the IMES can rely on the local energy provided by
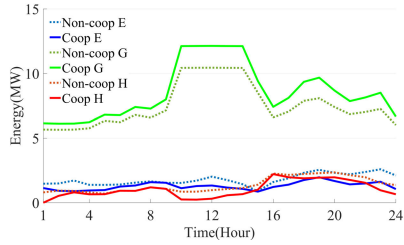
FIGURE 11. Purchased energy of the IMES.

TABLE 4. Detail operating costs.

Energy	Non-cooperation ($)	Cooperation ($)
Electricity	1898.78	1086.37
Gas	3313.62	3675.86
Heat	328.21	187.18

neighboring EHs to serve some of their energy demands and realize a higher utilization rate of RES.

The hourly operating costs is shown in Fig. 12. The cooperative operation outperforms the non-cooperation in terms of overall operating costs, as shown in Table 5. In addition, the operating costs of the R-EH1, the R-EH2, and the C-EH are lower because of the cooperation and internal energy exchange. However, the operating costs of the R-EH3 and the I-EH are increased. That this because the CHPs of the R-EH3 and the I-EH increase their energy output to compensate for the energy shortage of other EHs. Instead of solving the scheduling problem for each downward individual EH, the total operating costs of the all involved EHs are taken into account in the upper ward IMES. The costs are reduced by 4.3% leading to a more efficient energy utilization.
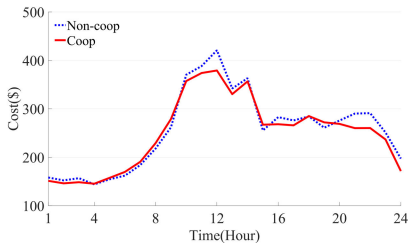

FIGURE 12. Operating costs of the IMES.

TABLE 5. Statistics of total operating costs of IMES.

Entity	Non-cooperation ($)	Cooperation ($)
R-EH1	1136.24	812.66
R-EH2	293.05	176.14
R-EH3	570.73	777.47
I-EH	2270.53	2508.23
C-EH	1969.88	1694.81
IMES	6240.43	5969.31

F. TRANSMISSION LOSS

Assume that the distance between the EHs of the IMES is depicted in Fig. 13. The extra heat and surplus electricity can be exchanged in the IMES.

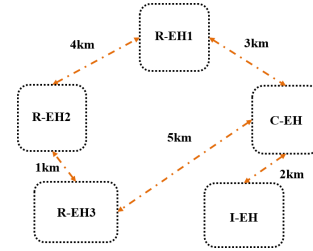As depicted in Fig. 14, the positive values mean that electricity and heat are inputted into an EH, and vice vasa.
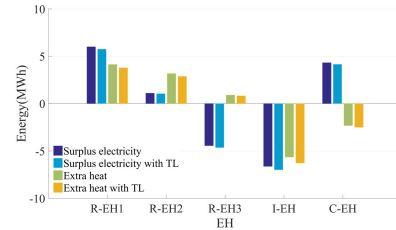

FIGURE 13. The diagram of IMES network.

FIGURE 14. The energy exchange in the IMES.

Taking C-EH as example, compared to the results without considering transmission loss (the dark blue and green bar in Fig. 14), the electricity input (the blue bar in Fig. 14) is slightly decreased and heat output (the yellow bar in Fig. 14) is increased due to the transmission loss (TL). The result illustrates that an EH with energy outputs needs to increase its energy supplies rather than simply meet the energy demands while the extra energy is used to compensate for the transmission loss. Because the imported energy cannot satisfy the internal energy demands due to the transmission loss, EHs who need external energy supplies will also request more internal energy supplies. The operating costs of each EH are summarized in Table 6. All EHs have higher operating costs when considering the transmission loss for electricity and heat.

TABLE 6. Statistics of total operating costs of IMES.

Entity	With TL ($)	Without TL ($)
R-EH1	839.24	812.66
R-EH2	184.29	176.14
R-EH3	794.93	777.47
I-EH	2583.53	2508.23
C-EH	1754.14	1694.81
IMES	6156.13	5969.31

V. CONCLUSION

To alleviate the pressure of energy depletion and enhance the multi-energy complementarity, this paper presented a cooperative operation model for the IMES with transmission losses. The energy distribution and conversion within the IMES were modeled using linear energy coupling matrices and energy flow equations. The operating costs are formulated as a multi-objective optimization problem based on the Pareto efficiency to obtain more diverse solutions. On this basis,

a novel multi-energy management strategy that integrates the alternative decomposition-based decoupling method for multi-energy flow and the DWPA was developed to optimizing the joint operating costs for the IMES. Compared with the non-cooperative operation mode, the case study demonstrates that the energy complementarity can improve the flexibility for energy systems and accommodate more RESs to reduce the power purchased from UG. Besides, with increasing confidence, the operating costs of the IMES increase. The proposed cooperative operation model and strategy can achieve more rational energy scheduling and better cost-effective performance, which can be further used in the optimization operation of energy internet.

REFERENCES

[1] L. Steg, R. Shwom, and T. Dietz, "What drives energy consumers?: Engaging people in a sustainable energy transition," *IEEE Power Energy Mag.*, vol. 16, no. 1, pp. 20–28, Jan. 2018.

[2] K. Zhou, S. Yang, and Z. Shao, "Energy Internet: The business perspective," *Appl. Energy*, vol. 178, pp. 212–222, Sep. 2016.

[3] J. Chen and Q. Zhu, "A game-theoretic framework for resilient and distributed generation control of renewable energies in microgrids," *IEEE Trans. Smart Grid*, vol. 8, no. 1, pp. 285–295, Jan. 2017.

[4] Q. Sun, Y. Zhang, H. He, D. Ma, and H. Zhang, "A novel energy function-based stability evaluation and nonlinear control approach for energy Internet," *IEEE Trans. Smart Grid*, vol. 8, no. 3, pp. 1195–1210, May 2017.

[5] Y. Wang, N. Zhang, Z. Zhuo, C. Kang, and D. Kirschen, "Mixed-integer linear programming-based optimal configuration planning for energy hub: Starting from scratch," *Appl. Energy*, vol. 210, pp. 1141–1150, Jan. 2018.

[6] S. D. Beigvand, H. Abdi, and M. La Scala, "A general model for energy hub economic dispatch," *Appl. Energy*, vol. 190, pp. 1090–1111, Mar. 2017.

[7] E. Kuznetsova, Y.-F. Li, C. Ruiz, and E. Zio, "An integrated framework of agent-based modelling and robust optimization for microgrid energy management," *Appl. Energy*, vol. 129, pp. 70–88, Sep. 2014.

[8] A. Ehsan and Q. Yang, "Optimal integration and planning of renewable distributed generation in the power distribution networks: A review of analytical techniques," *Appl. Energy*, vol. 210, pp. 44–59, Jan. 2018.

[9] S. Mashayekh, M. Stadler, G. Cardoso, M. Heleno, S. C. Madathil, H. Nagarajan, R. Bent, M. Mueller-Stoffels, X. Lu, and J. Wang, "Security-constrained design of isolated multi-energy microgrids," *IEEE Trans. Power Syst.*, vol. 33, no. 3, pp. 2452–2462, May 2018.

[10] A. Ehsan, Q. Yang, and M. Cheng, "A scenario-based robust investment planning model for multi-type distributed generation under uncertainties," *IET Gener., Transmiss. Distrib.*, vol. 12, no. 20, pp. 4426–4434, Nov. 2018.

[11] A. Ehsan and Q. Yang, "Coordinated investment planning of distributed multi-type stochastic generation and battery storage in active distribution networks," *IEEE Trans. Sustain. Energy*, vol. 10, no. 4, pp. 1813–1822, Oct. 2019.

[12] M. Yazdani-Damavandi, N. Neyestani, G. Chicco, M. Shafie-Khah, and J. P. S. Catalao, "Aggregation of distributed energy resources under the concept of multienergy players in local energy systems," *IEEE Trans. Sustain. Energy*, vol. 8, no. 4, pp. 1679–1693, Oct. 2017.

[13] G. Li, R. Zhang, T. Jiang, H. Chen, L. Bai, and X. Li, "Security-constrained bi-level economic dispatch model for integrated natural gas and electricity systems considering wind power and power-to-gas process," *Appl. Energy*, vol. 194, pp. 696–704, May 2017.

[14] A. Ehsan and Q. Yang, "Scenario-based investment planning of isolated multi-energy microgrids considering electricity, heating and cooling demand," *Appl. Energy*, vol. 235, pp. 1277–1288, Feb. 2018.

[15] I. Goroohi Sardou, M. E. Khodayar, and M. T. Ameli, "Coordinated operation of natural gas and electricity networks with microgrid aggregators," *IEEE Trans. Smart Grid*, vol. 9, no. 1, pp. 199–210, Jan. 2018.

[16] Y. Wang, J. Cheng, N. Zhang, and C. Kang, "Automatic and linearized modeling of energy hub and its flexibility analysis," *Appl. Energy*, vol. 211, pp. 705–714, Feb. 2018.

[17] K. Qu, T. Yu, L. Huang, B. Yang, and X. Zhang, "Decentralized optimal multi-energy flow of large-scale integrated energy systems in a carbon trading market," *Energy*, vol. 149, pp. 779–791, Apr. 2018.

[18] E. Dall'Anese, P. Mancarella, and A. Monti, "Unlocking flexibility: Integrated optimization and control of multienergy systems," *IEEE Power Energy Mag.*, vol. 15, no. 1, pp. 43–52, Jan. 2017.

[19] Y. Li, Y. Zou, Y. Tan, Y. Cao, X. Liu, M. Shahidehpour, S. Tian, and F. Bu, "Optimal stochastic operation of integrated low-carbon electric power, natural gas, and heat delivery system," *IEEE Trans. Sustain. Energy*, vol. 9, no. 1, pp. 273–283, Jan. 2018.

[20] M. Salehimaleh, A. Akbarimajd, K. Valipour, and A. Dejamkhooy, "Generalized modeling and optimal management of energy hub based electricity, heat and cooling demands," *Energy*, vol. 159, no. 15, pp. 669–685, Sep. 2018.

[21] Z. Jiang, R. Hao, Q. Ai, Z. Yu, and F. Xiao, "Extended multi-energy demand response scheme for industrial integrated energy system," *IET Gener., Transmiss. Distrib.*, vol. 12, no. 13, pp. 3186–3192, Jul. 2018.

[22] N. Holjevac, T. Capuder, N. Zhang, I. Kuzle, and C. Kang, "Corrective receding horizon scheduling of flexible distributed multi-energy microgrids," *Appl. Energy*, vol. 207, no. 1, pp. 176–194, Dec. 2017.

[23] A. Heidari, S. S. Mortazavi, and R. C. Bansal, "Stochastic effects of ice storage on improvement of an energy hub optimal operation including demand response and renewable energies," *Appl. Energy*, vol. 261, no. 1, Mar. 2020, Art. no. 114393.

[24] M. Roustaei, T. Niknam, S. Salari, H. Chabok, M. Sheikh, A. Kavousi-Fard, and J. Aghaei, "A scenario-based approach for the design of smart energy and water hub," *Energy*, vol. 195, no. 1, Mar. 2020, Art. no. 116931.

[25] H. Zafarani, S. A. Taher, and M. Shahidehpour, "Robust operation of a multicarrier energy system considering EVs and CHP units," *Energy*, vol. 192, no. 1, Feb. 2020, Art. no. 116703.

[26] Y. Li, B. Feng, G. Li, J. Qi, D. Zhao, and Y. Mu, "Optimal distributed generation planning in active distribution networks considering integration of energy storage," *Appl. Energy*, vol. 210, no. 15, pp. 1073–1081, Jan. 2018.

[27] Y. Zheng, D. J. Hill, and Z. Y. Dong, "Multi-agent optimal allocation of energy storage systems in distribution systems," *IEEE Trans. Sustain. Energy*, vol. 8, no. 4, pp. 1715–1725, Oct. 2017.

[28] S. F. Santos, D. Z. Fitiwi, A. W. Bizuayehu, M. Shafie-khah, M. Asensio, J. Contreras, C. M. P. Cabrita, and J. P. S. Catalao, "Novel multi-stage stochastic DG investment planning with recourse," *IEEE Trans. Sustain. Energy*, vol. 8, no. 1, pp. 164–178, Jan. 2017.

[29] C. Shao, X. Wang, M. Shahidehpour, X. Wang, and B. Wang, "An MILP-based optimal power flow in multicarrier energy systems," *IEEE Trans. Sustain. Energy*, vol. 8, no. 1, pp. 239–248, Jan. 2017.

[30] J. Liu, A. Wang, Y. Qu, and W. Wang, "Coordinated operation of multi-integrated energy system based on linear weighted sum and grasshopper optimization algorithm," *IEEE Access*, vol. 6, pp. 42186–42195, Jun. 2018.

[31] J. H. Zheng, Q. H. Wu, and Z. X. Jing, "Coordinated scheduling strategy to optimize conflicting benefits for daily operation of integrated electricity and gas networks," *Appl. Energy*, vol. 192, pp. 370–381, Apr. 2017.

[32] S. Fan, Z. Li, J. Wang, L. Piao, and Q. Ai, "Cooperative economic scheduling for multiple energy hubs: A bargaining game theoretic perspective," *IEEE Access*, vol. 6, pp. 27777–27789, May 2018.

[33] A. Lorestani and M. M. Ardehali, "Optimal integration of renewable energy sources for autonomous tri-generation combined cooling, heating and power system based on evolutionary particle swarm optimization algorithm," *Energy*, vol. 145, no. 15, pp. 839–855, Feb. 2018.

[34] C. Lin, W. Wu, B. Zhang, and Y. Sun, "Decentralized solution for combined heat and power dispatch through benders decomposition," *IEEE Trans. Sustain. Energy*, vol. 8, no. 4, pp. 1361–1372, Oct. 2017.

[35] X. Liu and P. Mancarella, "Modelling, assessment and sankey diagrams of integrated electricity-heat-gas networks in multi-vector district energy systems," *Appl. Energy*, vol. 167, no. 1, pp. 336–352, Apr. 2016.

[36] A. Zlotnik, L. Roald, S. Backhaus, M. Chertkov, and G. Andersson, "Coordinated scheduling for interdependent electric power and natural gas infrastructures," *IEEE Trans. Power Syst.*, vol. 32, no. 1, pp. 600–610, Jan. 2017.

[37] Z. Pan, Q. Guo, and H. Sun, "Interactions of district electricity and heating systems considering time-scale characteristics based on quasi-steady multi-energy flow," *Appl. Energy*, vol. 167, no. 1, pp. 230–243, Apr. 2016.

[38] A. Bostan, M. S. Nazar, M. Shafie-khah, and J. P. S. Catalão, "Optimal scheduling of distribution systems considering multiple downward energy hubs and demand response programs," *Energy*, vol. 190, no. 1, Jan. 2020, Art. no. 116349.

[39] S. Chen and S. Wang, "An optimization method for an integrated energy system scheduling process based on NSGA-II improved by tent mapping chaotic algorithms," *Processes*, vol. 8, no. 4, p. 426, Apr. 2020.

[40] Y. Wang, F. Li, H. Yu, Y. Wang, C. Qi, J. Yang, and F. Song, "Optimal operation of microgrid with multi-energy complementary based on moth flame optimization algorithm," *Energy Sources, A, Recovery, Utilization, Environ. Effects*, vol. 42, no. 7, p. 426, Mar. 2020.

[41] J. J. Grainger and W. D. Stevenson, *Power System Analysis*. New York, NY, USA: McGraw-Hill, 1994.

[42] M. Abeysekera, J. Wu, N. Jenkins, and M. Rees, "Steady state analysis of gas networks with distributed injection of alternative gas," *Appl. Energy*, vol. 164, no. 15, pp. 991–1002, Feb. 2016.

[43] X. Liu, "Combined analysis of electricity and heat networks," Ph.D. dissertation, Cardiff Univ., Cardiff, Wales, 2013.

[44] H.-S. Wu and F.-M. Zhang, "Wolf pack algorithm for unconstrained global optimization," *Math. Problems Eng.*, vol. 2014, pp. 1–17, Mar. 2014.

[45] A. F. Kamaruzaman, A. M. Zain, S. M. Yusuf, and A. Udin, "Levy flight algorithm for optimization Problems–A literature review," *Appl. Mech. Mater.*, vol. 421, pp. 496–501, Sep. 2013.

[46] S. You and Q. Peng, "A non-convex alternating direction method of multipliers heuristic for optimal power flow," in *Proc. IEEE Int. Conf. Smart Grid Commun. (SmartGridComm)*, Venice, Italy, Nov. 2014, pp. 788–793.

[47] F. Li, J. Qin, and W. X. Zheng, "Distributed Q-learning-based online optimization algorithm for unit commitment and dispatch in smart grid," *IEEE Trans. Cybern.*, early access, Jun. 26, 2019, doi: 10.1109/TCYB.2019.2921475.

[48] B. Huang, C. Zheng, Q. Sun, and R. Hu, "Optimal economic dispatch for integrated power and heating systems considering transmission losses," *Energies*, vol. 12, no. 13, p. 2502, Jun. 2019.

CHONGHUI SONG received the B.S. degree in fluid machine engineering from Xi'an Jiaotong University, Xi'an, China, in 1996, and the M.S. and Ph.D. degrees in automatic control theory and engineering from Northeastern University, Shenyang, China, in 1999 and 2004, respectively. From 2006 to 2008, he was a Visiting Scholar with the Department of Electrical and Computer Engineering, University of Illinois at Chicago. He is currently an Associate Professor with the College of Information Science and Engineering, Northeastern University. His current research interests include computational intelligence, intelligent control, differential game, optimal control, and dynamic programming.

JINGLU LIU received the B.S. degree in electrical engineering automation from Hohai University, in 2013, and the M.S. degree in measurement technology and instruments from Northeastern University, China, in 2015, where he is currently pursuing the Ph.D. degree in power electronics and drives with the School of Information Science and Engineering. His current research interests include distributed energy optimization and its applications in energy systems, smart grid, and energy internet.

ANNA WANG received the B.S., M.S., and Ph.D. degrees in measurement technology and instruments from Northeastern University, Shenyang, China, in 1982, 1988, and 2001, respectively. Since 1994, she has been a Full Professor and a Ph.D. Supervisor with the School of Information Science and Engineering, Northeastern University, China. Her main research interests include analysis and diagnosis of electrical equipment and power systems, optimization analysis technology of smart grid, and electric network control of distributed generation systems.

RAN TAO is currently pursuing the degree with the Faculty of Engineering and Information Technologies, The University of Sydney, Australia. His current research interests include distributed renewable energy resources optimization and its applications in microgrids, smart grid, and energy converting.

XINGYU WANG received the B.S. degree in electrical engineering and automation and the M.S. degree in electrical engineering from Liaoning Technical University, Liaoning, China, in 2014 and 2017, respectively. He is currently pursuing the Ph.D. degree in power electronics and power drives with Northeastern University, Liaoning. His research interests include power electronic technology and basic theory of electrical equipment.

• • •